


## Vibrational quenching and reactive processes of weakly bound molecular ions colliding with atoms at cold temperatures

Jesús Pérez-Ríos

*School of Natural Sciences and Technology, Universidad del Turabo, Gurabo, Puerto Rico 00778, USA*

 (Received 2 July 2018; revised manuscript received 13 September 2018; published 19 February 2019)

We present a study about vibrational quenching and chemical processes of cold molecular ions immersed in an ultracold atomic gas. In particular, the quasiclassical trajectory method is applied to  $\text{BaRb}^+(v) + \text{Rb}$  collisions at  $T \gtrsim 1$  mK, revealing a large vibrational quenching cross section, which follows the Langevin capture model prediction. These results play a key role in the understanding of relaxation phenomena of cold molecular ions in ultracold gases.

DOI: [10.1103/PhysRevA.99.022707](https://doi.org/10.1103/PhysRevA.99.022707)

### I. INTRODUCTION

Cold hybrid ion-neutral systems are a unique playground for understanding cold chemistry [1–3], the design of high precision spectroscopy techniques [4], and the development of effective quantum logic spectroscopy approaches [5–7]. Moreover, these systems are suitable for engineering quantum information protocols [8–10] as well as for the simulation of complex many-body Hamiltonians [11–13]. In cold chemistry, the major driving force is the study of molecular ions colliding with neutrals. Those studies could elucidate the ultimate nature of ion-neutral collisions including stereochemical effects, the possibility of sympathetic cooling of molecular ions with neutrals, and the development of rotational spectroscopy techniques for molecular ions [4,14,15]. These applications rely on the control of the internal degrees of freedom of the molecular ion. However, molecular ion-neutral collisions lead to a decoherence process, known as relaxation, that depends on the collision energy, in which the kinetic energy is effectively transferred to the internal degrees of freedom of the molecular ion (rotation and vibration) and vice versa.

Relaxation has extensively been studied in chemical physics [16–19]. In particular, for neutral species at room temperature, although recently, some efforts have been devoted to the study of rotational and vibrational relaxation of molecular ions in ultracold gases. These studies focused on vibrational and rotational relaxation of deeply bound vibrational states [20–26]. However, three-body recombination of ions in a highly dense ultracold gas leads to an efficient production of highly excited vibrational molecular ions [27,28]. In this scenario, relaxation mechanisms remain unexplored.

In this paper, we present the study of vibrational relaxation and reactive processes of highly excited vibrational molecular ions in a neutral gas at cold temperatures. In particular, we will study  $\text{BaRb}^+ - \text{Rb}$  collisions, which are relevant after a single  $\text{Ba}^+$  is brought in contact with a dense cloud of ultracold Rb atoms [27]. Our theoretical approach is based on quasiclassical trajectory (QCT) method fueled by the satisfactory results of classical trajectory calculations for ion-neutral-neutral three-body recombination [27,29].

The paper is structured as follows: in Sec. II the QCT method for molecular ion-neutral collisions is introduced. Next, this theoretical approach is applied to  $\text{BaRb}^+ - \text{Rb}$ , and the results for vibrational quenching and different chemical reactive channels are presented in Sec. III. Finally, in Sec. IV a brief summary and conclusions are presented.

### II. QUASICLASSICAL TRAJECTORY (QCT) CALCULATIONS

QCT is a well-established technique in chemical physics since the pioneering work of Karplus *et al.* for the study of the H exchange reaction in  $\text{H}_2 - \text{H}$  [30,31]. In this approach, the dynamics of the nuclei in the potential-energy surface (PES) follows Newton's laws. The initial point of a trajectory is randomly chosen such that the energy of the molecule coincides with its rovibrational energy through the Wentzel, Kramers, and Brillouin (WKB) or semiclassical quantization rule. At the final point of propagation, the WKB quantization rule applies to lead to the final rovibrational state of the molecule.

The Hamiltonian of three interacting particles under the potential-energy surface  $V(\vec{r}_1, \vec{r}_2, \vec{r}_3)$  is better described in Jacobi coordinates [29,31,32] shown in Fig. 1. In particular, neglecting the trivial center-of-mass (c.m.) motion one finds

$$H = \frac{\vec{P}_1^2}{2m_{12}} + \frac{\vec{P}_2^2}{2m_{3,12}} + V(\vec{\rho}_1, \vec{\rho}_2), \quad (1)$$

with  $m_{12} = (m_1^{-1} + m_2^{-1})^{-1}$  and  $m_{3,12} = (m_3^{-1} + m_{12}^{-1})^{-1}$ . Here  $\vec{\rho}_1$  represents the Jacobi vector describing the molecule position,  $\vec{P}_1$  stands for its conjugate momentum, whereas  $\vec{\rho}_2$  stands for the motion of the atom with respect to the center of mass of the molecule and  $\vec{P}_2$  is its momentum.

The motion of the nuclei is tracked by solving Hamilton's equations of motion, which in this case are

$$\frac{d\rho_{i,\alpha}}{dt} = \frac{\partial H}{\partial P_{i,\alpha}}, \quad (2)$$

$$\frac{dP_{i,\alpha}}{dt} = -\frac{\partial H}{\partial \rho_{i,\alpha}}, \quad (3)$$

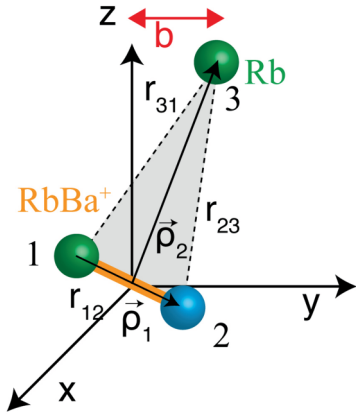


FIG. 1. Schematic of atom-molecule collision: impact parameter  $b$ , Jacobi vectors ( $\vec{\rho}_1$ ,  $\vec{\rho}_2$ ), and its relation with the interatomic vectors  $\vec{r}_{ij}$ , with  $(i, j) = 1, 2, 3$  and  $i \neq j$ .

where  $i = 1, 2$  and  $\alpha$  denotes the different Cartesian components of the Jacobi vectors.

### A. Initial conditions

Let us assume an atom-molecule collision with a given collision energy  $E_k$  in the c.m. frame, where the atom is placed along the  $z$  axis at a given distance  $R$  from the c.m. of the molecule, positioned at the origin of the coordinate system (see Fig. 1). In this case, after specifying the impact parameter  $b$  the vectors  $\vec{\rho}_2$  and  $\vec{P}_2$  are fully characterized [31]. On the other hand, the initial rovibrational state  $(v, j)$  of the molecule specifies  $\vec{\rho}_1$  and  $\vec{P}_1$ . The size of the molecule  $|\rho_1|$  is given by the outer classical turning point  $r_+$  of the rovibrational motion, whereas  $P_1 = \hbar j(j+1)/r_+$ , with  $j$  being the rotational quantum number. Finally, the orientation of these vectors are randomly chosen by sampling the azimuthal angle  $\theta$  of the molecule with respect to the  $z$  axis, its polar angle in the  $x - y$  plane  $\phi$  and the angle  $\eta$  between the angular momentum of the molecule  $\vec{J} = \vec{\rho}_1 \times \vec{P}_1$  and a normal vector to the molecular axis.

Finally, to fully randomize rotation and vibration of the molecule in each collision, one needs to choose properly the initial distance between the incoming particle and the target  $R = R_0 + \frac{\chi P_2 \tau_{v,j}}{\mu_{3,12}}$  ( $R = |\vec{\rho}_2|$ ), where  $R_0$  is some fixed atom-molecule distance in which the potential energy is negligible in comparison with the collision energy,  $\chi \in [0, 1]$  is a uniform random variable, and

$$\tau_{v,j} = \sqrt{2m_{12}} \int_{r_-}^{r_+} \frac{dr}{\sqrt{E_{\text{int}} - V(r) - \frac{\hbar^2 j(j+1)}{2m_{12}r^2}}} \quad (4)$$

is the vibrational period. In Eq. (4),  $E_{\text{int}}$  represents the rovibrational energy and  $V(r)$  stands for the molecular potential-energy curve [33], and  $r_-$  represents the inner classical turning point for the given rovibrational energy of the molecule.

### B. Reaction products

Here, we consider three different product states for a molecular ion-atom collision [34].

(i) Quenching ( $q$ ):  $\text{AB}^+(v) + \text{C} \rightarrow \text{AB}^+(v') + \text{C}$ . A change of the rovibrational state of the molecular ion, whose vibrational quantum number is given by

$$v' = -\frac{1}{2} + \frac{1}{\pi \hbar} \int_{r_-}^{r_+} \sqrt{2m_{12} \left[ E_{\text{int}} - V(r) - \frac{\hbar^2 j'(j'+1)}{2m_{12}r^2} \right]} dr, \quad (5)$$

where  $E'_{\text{int}}$  represents the internal energy of the molecule and  $j'$  is the rotational quantum number given by  $j' = -1/2 + 1/2\sqrt{1 + 4\vec{J}' \cdot \vec{J}'/\hbar^2}$ , where  $\vec{J}' = \vec{\rho}_1 \times \vec{P}_1$  at the final propagation time. The value of  $v'$  obtained from Eq. (5) is rounded to the closest integer number, which is the so-called standard binding method [31]. However, some other binding techniques are available, such as the celebrated Gaussian binning method, which relies on a Gaussian weighting of the trajectories with respect the integer  $v'$  value [35].

(ii) Dissociation ( $d$ ): three free atoms as a final state,  $\text{AB}^+(v) + \text{C} \rightarrow \text{A} + \text{B}^+ + \text{C}$ . This process becomes operative when the collision energy is larger than the binding energy of the molecular ion. These events are computationally detected when the three interatomic energies between the pairs of atoms are positive.

(iii) Reaction ( $r$ ): formation of a new product not present in the reactants,  $\text{AB}^+(v) + \text{C} \rightarrow \text{CB}^+(v'') + \text{A}$  and  $\text{AB}^+(v) + \text{C} \rightarrow \text{AC}(v''') + \text{B}^+$ . This is identified by looking at the internal energy of the atom pairs in the system and searching which is negative. Then, by applying Eq. (5) with the right interatomic potential and reduced mass, the vibrational and rotational level of the product state can be addressed.

### C. Cross section

The classical cross section associated with any of the processes exposed above is

$$\sigma_{q,r,d}(E_k) = 2\pi \int_0^{b_{\text{max}}^{q,r,d}(E_k)} P_{q,r,d}(b, E_k) b db, \quad (6)$$

where  $b_{\text{max}}^{q,r,d}(E_k)$  indicates the maximum impact parameter for trajectories leading to the process at hand and  $P_{q,r,d}(b, E_k)$  is the opacity function. The opacity function represents the probability of a given process ( $q$ ,  $r$ , or  $d$ ) as a function of the impact parameter  $b$  and collision energy as

$$P_{q,r,d}(b, E_k) = \int P_{q,r,d}(b, E_k, \theta, \phi, \eta, \xi) d\Omega \quad (7)$$

$$d\Omega = \sin \theta d\theta d\phi d\eta d\xi.$$

This integral is evaluated through Monte Carlo sampling leading to

$$P_{q,r,d}(b, E_k) = \frac{N_{q,r,d}(b, E_k)}{N} \pm \delta_{q,r}(b, E_k), \quad (8)$$

where  $N_{q,r,d}(b, E_k)$  denotes the number of trajectories associated with the process of interest and  $N$  stands for the total number of trajectories launched for a given  $b$  and  $E_k$ . Here,

$$\delta_{q,r,d}(b, E_k) = \frac{\sqrt{N_{q,r,d}(b, E_k)}}{N} \sqrt{\frac{N - N_{q,r,d}(b, E_k)}{N}} \quad (9)$$

stands for the standard deviation of the opacity function.

### D. Validity of QCT

QCT is an approximation to the realistic quantum nature of a collision event and therefore is applicable under certain conditions. In particular, QCT describes quantitatively the scattering observables when many partial waves are involved. However, QCT cannot predict resonances since the dynamics is carried out classically.

Here, we assume that the QCT approach is applicable for  $l \gtrsim 20$ , where  $l$  is the number of partial waves involved in the scattering problem at hand. At  $l = 20$  it is very probable that most scattering systems will show many resonances (this is even more clear in the case of heavy colliding partners, as in our case), and hence we chose it as a tentative value for describing a lower bound of the validity region of QCT. However, this criterion depends on the collision energy and more profoundly on the interaction potential. For a general long-range interaction potential  $-C_n/r^n$ , with  $n \geq 3$  and a given collision energy  $E_k$ , the largest classically allowed partial wave is given by

$$l = \left( \frac{2}{n-2} \right)^{\frac{n-2}{2n}} \sqrt{n} E_k^{\frac{n-2}{2n}} C_n^{1/n} \mu^{1/2}, \quad (10)$$

where  $\mu$  is the reduced mass of the colliding partners. This equation reveals the expected number of partial waves that significantly contribute to the scattering at a given collision energy. Then, by choosing a particular value of  $l$  we solve Eq. (10) for the collision energy, leading to the lowest energy where the QCT approach is reliable.

In Fig. 2 it is shown the range of validity of QCT for alkali-metal-alkali-metal and alkali-metal-alkali-metal ion collisions, assuming  $l = 20$  in Eq. (10). As a result, one notices that for ion-neutral collisions QCT may be applicable up to collision energies  $\sim 1$  mK, whereas in the case of neutral neutral is  $\sim 1$  K. This discrepancy clearly reflects the role of the long-range interaction of the system. In particular, for

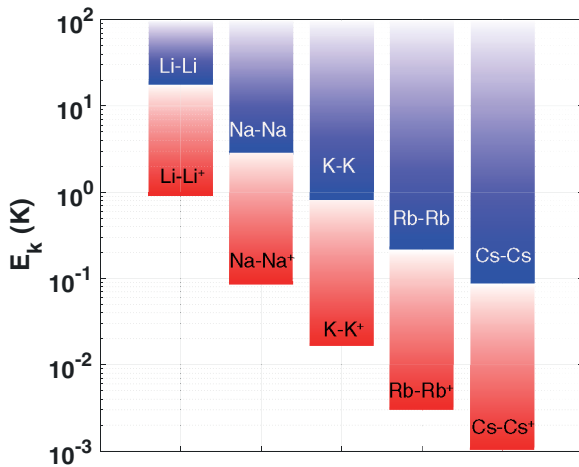


FIG. 2. Validity region of the QCT approach for different alkali-metal-alkali-metal and alkali-metal-alkali-metal ion collisions. The red bottom of the bars represents the lowest collision energy where QCT is applicable for ion-neutral collisions, whereas the dark blue region represents the same but for neutral-neutral collisions. The range of applicability of QCT does not have an upper limit, independent of the kind of interaction.

BaRb<sup>+</sup>-Rb at 1 mK we will need to include up to 18 partial waves. Thus QCT is a reasonable approach for  $T \gtrsim 1$  mK.

### III. RESULTS

We run batches of  $10^4$  trajectories per collision energy covering 100 values of the impact parameter, i.e.,  $N = 100$ . The trajectories were propagated by solving Eqs. (2) and (3) through the Cash-Karp Runge-Kutta method [36] leading to the conservation of the total energy to at least four significant digits while the total angular momentum,  $J = |\vec{\rho}_1 \times \vec{P}_1 + \vec{\rho}_2 \times \vec{P}_2|$ , is conserved to at least six digits. In our approach, we assume that the three-body potential-energy surface can be described through pairwise additive potentials as  $V(\vec{r}_1, \vec{r}_2, \vec{r}_3) = V(\vec{r}_{12}) + V(\vec{r}_{13}) + V(\vec{r}_{23})$  (see Fig. 1).

Here we focus on the physical scenario described in Refs. [3,27], in which the Rb atoms are spin polarized. Therefore, they interact through their triplet potential which is taken from Ref. [37]. For the Ba<sup>+</sup>-Rb interaction it is assumed that the charge is localized in the Ba atom and the interatomic interaction is described by means of the generalized Lennard-Jones potential:  $V(r) = -C_4/r^4[1 - 1/2(r_m^4/r^4)]$ , where  $r$  is the atom-ion distance [38],  $C_4 = 160$  a.u., and  $r_m = 9.27a_0$ . Moreover, we assume that the spin of the ion is also polarized; thus this scenario corresponds with the triplet potential-energy curve for the BaRb<sup>+</sup> system. In Fig. 3 is shown the present PES of the system at hand.

The vibrational states closer to dissociation for BaRb<sup>+</sup> based on our model potential are shown in Table I. With our model we reproduce properly the progression and density of vibrational states, since we employ the physical long-range interaction. However, the number and energy of bound states are not the physical ones.

In Fig. 4 some trajectories associated with the collision BaRb<sup>+</sup>( $v$ ) + Rb are shown. Here one notices that the trajectory shown in panel (b) leads to a dissociation process,

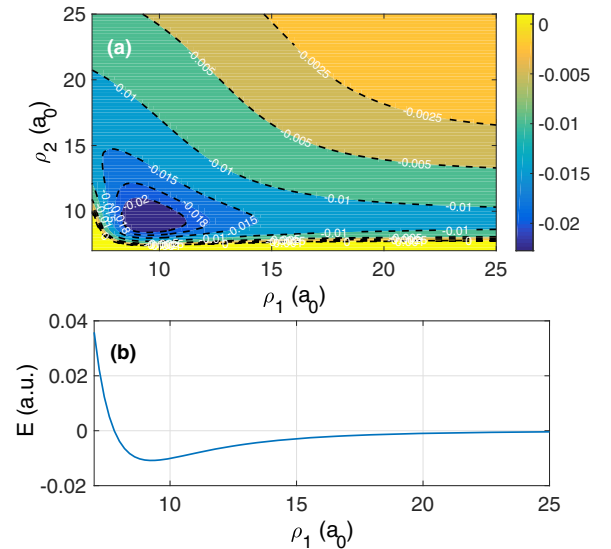


FIG. 3. Potential-energy surface for BaRb<sup>+</sup>-Rb as a function of the magnitude of the Jacobi coordinates (see Fig. 1). Panel (a) shows the contour plot of the PES employed in this work for the equilibrium angle between the Jacobi vectors at the global minimum. The employed BaRb<sup>+</sup> PEC is presented in panel (b).

TABLE I. Vibrational bound states for  $\text{BaRb}^+$  (in mK) assuming the generalized Lenard-Jones potential described in the text.

$v$	Binding energy ( $E_v$ )
198	0.01
197	0.11
196	0.43
195	1.13
194	2.48
193	4.77
192	8.37
191	13.70
190	21.24
189	31.52
188	45.15
187	62.84
186	85.12
185	113.03

whereas the trajectories of panels (a) and (c) correspond to quenching events. In these trajectories the initial  $\text{BaRb}^+$  molecule shows a large outer point, which is characteristic of shallow bound states in potentials with  $1/r^4$ . However, we would like to stress that the trajectory of panel (c) shows a more intriguing situation: after an initial molecular ion-neutral event the two neutrals and the ion form a trimer during 10 ns that finally decays into  $\text{BaRb}^+(v') + \text{Rb}$ , resembling the so-called roaming resonances [39]. Also, it is worth pointing out that the exchange reaction shown in panel (c) is counted as an inelastic event rather than a reactive one, owing to the quantal indistinguishability of the atoms.

### A. Vibrational quenching cross section

Figure 5 shows the quenching cross section for  $\text{RbBa}^+(v) + \text{Rb}$  as a function of the initial vibrational state ( $v = 187-195$ ) at different collision energies. The results have been obtained through numerical integration of Eq. (6) by

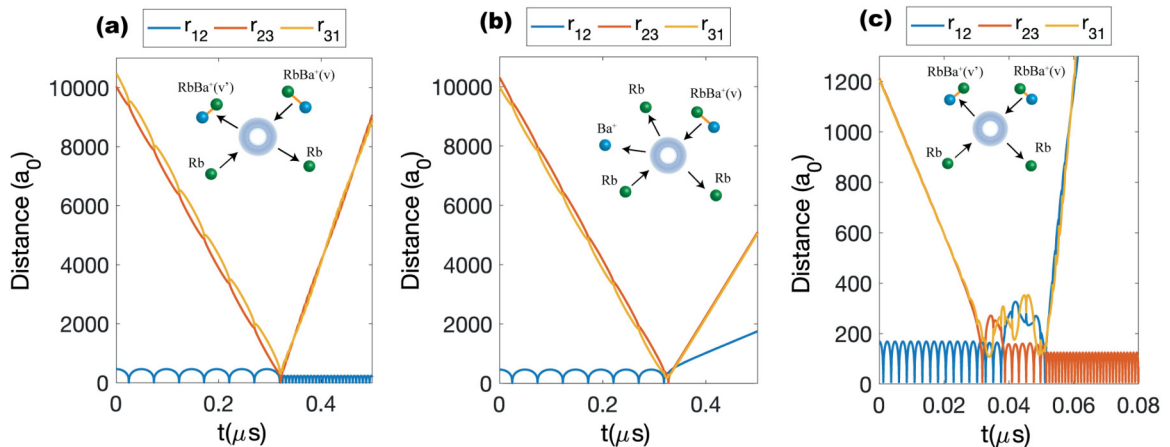


FIG. 4. Trajectories for  $\text{RbBa}^+(v) + \text{Rb}$  collisions. Panel (a): trajectory for  $b = 0a_0$ ,  $v = 195$ , and  $E_k = 10$  mK leading to a quenching process where  $v' = 191$ . Panel (b): a trajectory for  $b = 90a_0$ ,  $v = 195$ , and  $E_k = 10$  mK leading to a dissociation process. Panel (c): a collision for  $b = 0a_0$ ,  $v = 187$ , and  $E_k = 10$  mK leading to a quenching collision with  $v' = 184$ . In this collision the quenching is produced through an exchange of the Rb atom leading to a quenching collision. The inset of each figure represents a scheme of the physical process under study.

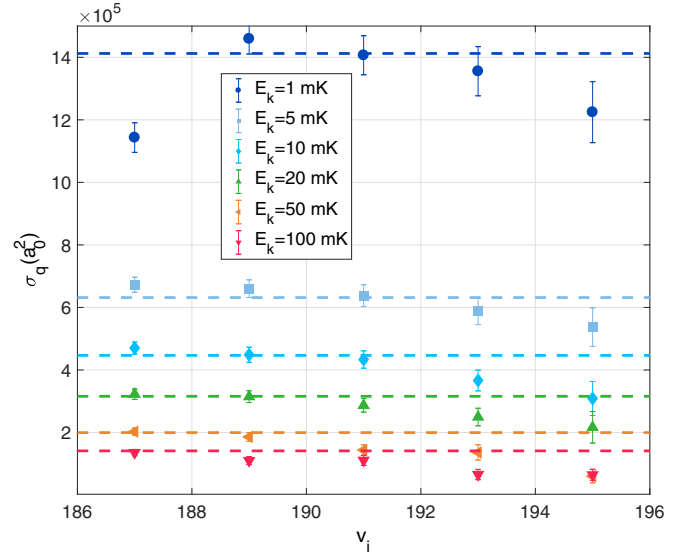


FIG. 5. Quenching cross section for the collision  $\text{BaRb}^+(v) + \text{Rb} \rightarrow \text{BaRb}^+(v' \neq v) + \text{Rb}$  as a function of the initial vibrational states (horizontal axis) and collision energy (denoted as the different symbols). The dashed lines represent the Langevin cross section for different collision energies. For these calculations we took  $j = 0$ . The error bars are related with one standard deviation of the opacity function [see Eq. (9) from the text].

means of the opacity function determined through the Monte Carlo sampling method. Here, one notices that the vibrational quenching cross section for a given collision energy is nearly independent of the initial vibrational state. Furthermore, the vibrational quenching cross section depends on the collision energy as  $E_k^{-1/2}$ , in agreement with the prediction of the Langevin capture model  $\sigma_L(E_k) = \pi(4C_4/E_k)^{1/2}$  (colored dashed lines in Fig. 5). However, for  $E_k \geq 10$  mK, some systematic small deviation between QCT predictions and the Langevin cross section is observed for  $v = 195$  and  $v = 193$ .

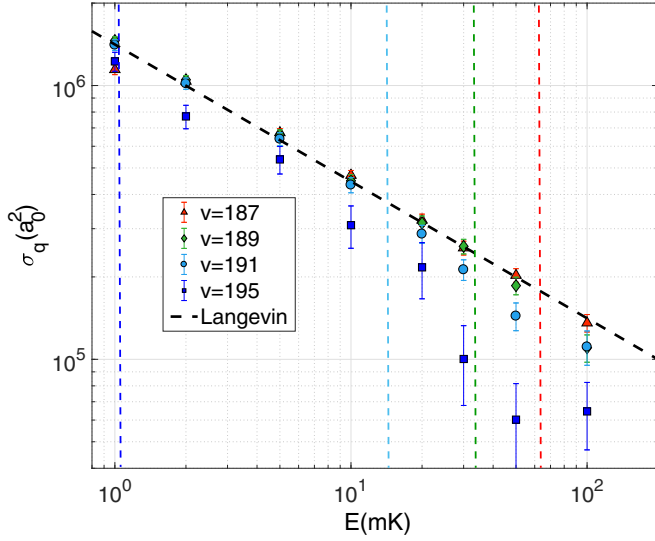


FIG. 6. Quenching cross section for  $\text{BaRb}^+(v) + \text{Rb} \rightarrow \text{BaRb}^+(v' \neq v) + \text{Rb}$  as a function of the collision energy  $E_k$ . The different initial vibrational states  $v$  are denoted by different symbols as indicated on the legend. The dashed thick line represents the Langevin cross section. For these calculations we took  $j = 0$ . The vertical dashed lines stand for the binding energy of the initial vibrational states of the molecular ion. The error bars are related with one standard deviation as introduced in Eq. (9).

In Fig. 6 we show the quenching cross section for  $\text{RbBa}^+(v) + \text{Rb}$  as a function of the collision energy. This figure shows that the quenching cross section for initial deeply bound molecular states agrees with the Langevin prediction, whereas for shallow vibrational states some discrepancies appear. In particular, shallower vibrational states start to deviate from the Langevin model at lower collision energies than more deeply bound vibrational states. These deviations are due to the presence of a new reaction channel: dissociation, since the collision energy is sufficient to break the molecular bond producing three free atoms.

### B. Dissociation cross section

Dissociation appears when the colliding Rb atom breaks the molecular bond of the molecular ion, i.e.,  $\text{BaRb}^+(v) + \text{Rb} \rightarrow \text{Ba}^+ + \text{Rb} + \text{Rb}$ . This channel is only accessible for  $E_k > E_v$ . The dissociation cross section as a function of the collision energy is shown in Fig. 7, where we see that only for  $E_k > E_v$  (see Table I) this channel becomes relevant for the dynamics. Also, we observe that the higher the collision energy the larger the cross section, reaching the Langevin prediction.

To further understand the efficiency of the energy transfer between translational and internal degrees of freedom we introduce the adiabaticity parameter  $\xi$  [40], which gives the efficiency of a given energy transfer process by comparing the relevant time scales. In the case at hand,  $\xi = \tau_c / \tau_{v,j}$ , where  $\tau_c$  [41] is the collision time and  $\tau_{v,j}$  is the vibrational period introduced in Sec. II A. Large values of  $\xi$  imply that the molecule vibrates many times before the collision happens,

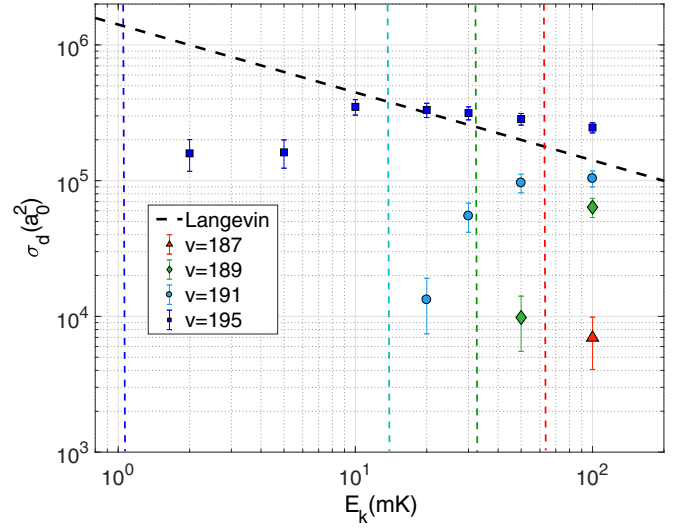


FIG. 7. Dissociation cross section for the collision  $\text{BaRb}^+(v) + \text{Rb} \rightarrow \text{Ba}^+ + \text{Rb} + \text{Rb}$  as a function of the collision energy  $E_k$ . The different initial vibrational states  $v$  are denoted by different symbols as indicated on the legend. The dashed thick line represents the Langevin cross section. The vertical dashed lines stand for the binding energy of the initial vibrational states of the molecular ion. For these calculations, we took  $j = 0$ .

which corresponds to an inefficient vibrational-translational energy transfer. For  $\xi \approx 1$  the energy transfer becomes efficient due to the synchronization between collision and vibration, but it is only when  $\xi \ll 1$  that the molecule shows a negligible vibrational motion during the collision and approaches to the high-efficiency energy transfer limit [40].

For the system at hand, we find that  $\xi \ll 1$  for all the relevant vibrational and collision energies studied. Therefore, vibrational quenching and dissociation processes should be efficient, as is revealed by the QCT calculations in Figs. 5, 6, and 7. In the particular case of dissociation, apart from being efficient, it needs to be energetically available, as the results of Fig. 7 demonstrate.

### C. Distribution of final states

The vibrational quenching cross section accounts for all the different trajectories leading to the molecular state with a different vibrational state; however, it does not provide information about the state-to-state processes. In other words, it does not say anything about the energy distribution of the product states. From the opacity function we have calculated the probability of finding the molecular ion in a given  $v'$  state [ $\text{BaRb}^+(v) + \text{Rb} \rightarrow \text{BaRb}^+(v' \neq v) + \text{Rb}$ ], and the results for different collision energies are shown in Fig. 8. In this figure, one notices a broad vibrational distribution of the final states, although a single quanta vibrational deexcitation is the most probable final state after a quenching process. In particular, in panel (a) at  $E_k = 1$  mK there is not an available excited vibrational state. In panel (b) at  $E_k = 10$  mK, some excited vibrational states for  $v = 193$  become available and they show a decent probability of 7% owing to the high efficiency vibrational energy transfer; the same applies in panel (c) with

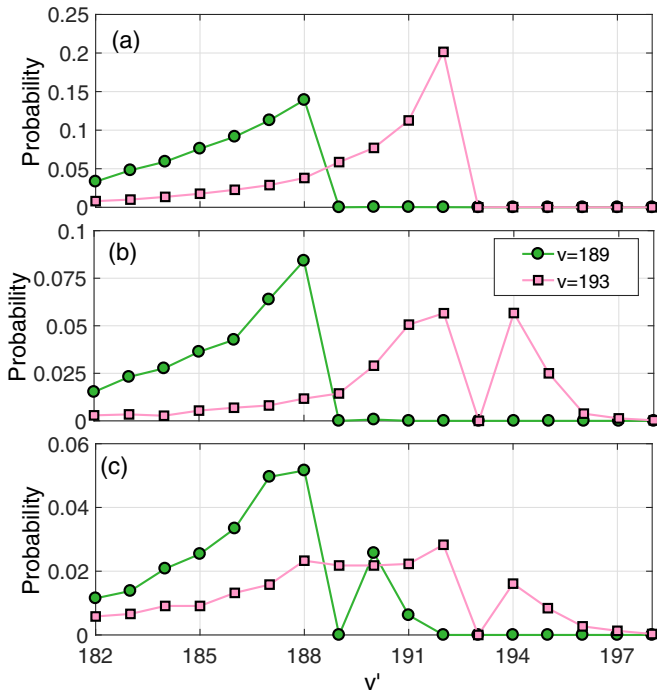


FIG. 8. Vibrational distribution for the product states after the quenching process  $\text{BaRb}^+(v) + \text{Rb} \rightarrow \text{BaRb}^+(v' \neq v) + \text{Rb}$  for different energies: panel (a)  $E_k = 1$  mK, panel (b)  $E_k = 10$  mK, and panel (c)  $E_k = 20$  mK.

$E_k = 20$  mK, but now some excited vibrational states are also available for  $v = 189$ . Also, it is worth observing that as the collision energy grows the overall amplitude of the vibrational distribution decreases due to the dissociation channel.

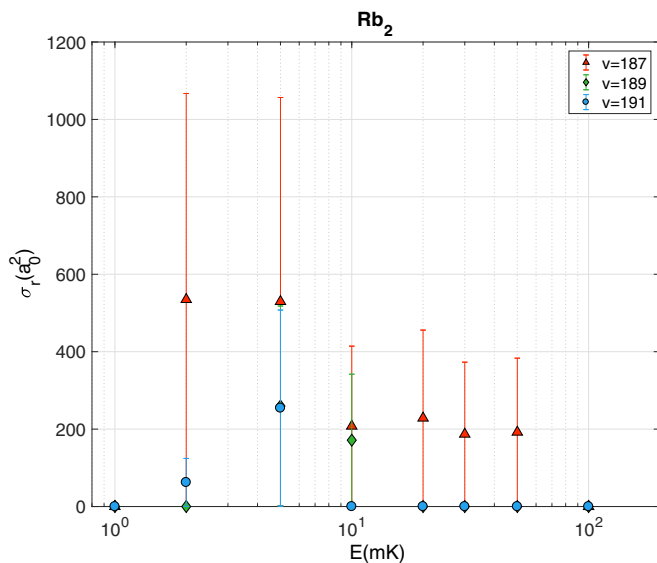


FIG. 9. Reaction cross section for the collision  $\text{BaRb}^+(v) + \text{Rb} \rightarrow \text{Rb}_2(v'') + \text{Ba}^+$  as a function of the collision energy  $E_k$ . The initial vibrational states  $v$  are denoted by symbols related to the initial vibrational states as indicated in the legend. For these calculations we took  $j = 0$ .

#### D. Reactive channel: $\text{Rb}_2$ as the final product state

The reactive process  $\text{BaRb}^+(v) + \text{Rb} \rightarrow \text{Rb}_2(v'') + \text{Ba}^+$  is a possible reaction pathway, which has been considered and the results for the cross section shown in Fig. 9. In this figure, it is noticed that the formation of  $\text{Rb}_2$  is  $\sim 10^3$  times less probable than vibrational quenching or dissociation (see Figs. 6 and 7), which confirms that the ion-neutral interaction is the dominant interaction of the system, as it was previously demonstrated for three-body recombination [27,28]. Therefore, we can conclude that in ion-atom-atom systems the ion prefers to form a molecule with a neutral than to be free after a molecular ion-atom collision. Nevertheless, from the figure, it is interesting to point out that for loosely bound vibrational states of the molecular ion the formation of  $\text{Rb}_2$  seems to be negligible. On the contrary, deeply bound states exhibit the opposite behavior. This may be related to the fact that the weakly bound vibrational states of neutral molecules show higher binding energies than their ionic analogs.

#### IV. CONCLUSIONS

We have shown that the QCT calculation method is a suitable tool to describe ion-neutral collisions for cold chemistry environments. In particular, we have focused on the study of vibrational quenching and dissociation of molecular ions in loosely bound vibrational states colliding with neutral atoms at cold temperatures.  $\text{BaRb}^+(v) + \text{Rb}$  has been chosen as the prototypical system due to its experimental relevance in ion-neutral-neutral three-body recombination experiments at cold temperatures. The validity of a quasiclassical approach has been shown for collision energies  $\gtrsim 1$  mK owing to the 18 partial waves that contribute to the cross section. As a result, we have shown that a QCT calculations-based vibrational quenching cross section follows the Langevin capture model independent of the vibrational state of the molecular ion; this translates into a very efficient energy transfer between translational and vibrational degrees of freedom.

Our study complements previous studies employing the coupled-channel method for vibrational quenching of molecular ions in deeply bound vibrational states colliding with ultracold atoms [20–25]. Indeed, using a coupled-channel approach here would be extremely computationally heavy due to the large size of the Hilbert space, as well as the large number of partial waves that must be included. Thus QCT seems to be a very good and reliable method for studying collisional processes of vibrationally excited molecular ions colliding with ultracold atoms. Finally, our results have implications in ion-neutral-neutral three-body recombination experiments, assisting in the understanding of the role of the trapping laser in the dynamics of the molecular ion [27], as well as its inherent importance in understanding the relaxation mechanism of cold molecular ions in an ultracold gas.

#### ACKNOWLEDGMENTS

We would like to acknowledge Amir Mohammadi and Johannes Denschlag for motivating this work through fruitful discussions and elucidating the experimental implications of our work, as well as Matthew T. Eiles and Francis Robicheaux for carefully reading the manuscript prior to publication.

- [1] M. Tomza, K. Jachymski, R. Gerritsma, A. Negretti, and T. Calarco, [arXiv:1708.07832v1](#).
- [2] S. Willitsch, M. T. Bell, A. D. Gingell, and T. P. Softley, *Phys. Chem. Chem. Phys.* **10**, 7200 (2008).
- [3] A. Härter and J. H. Denschlag, *Contemp. Phys.* **55**, 33 (2014).
- [4] S. Brünken, L. Kluge, A. Stoffels, J. Pérez-Ríos, and S. Schlemmer, *J. Mol. Spectrosc.* **332**, 67 (2017).
- [5] J. Mur-Petit, J. J. García-Ripoll, J. Pérez-Ríos, J. Campos-Martínez, M. I. Hernández, and S. Willitsch, *Phys. Rev. A* **85**, 022308 (2012).
- [6] D. Leibfried, *New J. Phys.* **14**, 023029 (2012).
- [7] F. Wolf, Y. Wang, J. C. Heip, F. Gebert, C. Shi, and P. O. Schmidt, *Nature (London)* **530**, 457 (2016).
- [8] S. Debnath, N. M. Linke, C. Figgatt, K. A. Landsman, K. Wright, and C. Monroe, *Nature (London)* **536**, 63 (2016).
- [9] H. Doerk, Z. Idziaszek, and T. Calarco, *Phys. Rev. A* **81**, 012708 (2010).
- [10] L.-M. Duan and C. Monroe, *Rev. Mod. Phys.* **82**, 1209 (2010).
- [11] J. Zhang, P. W. Hess, A. Kyprianidis, P. Becker, A. Lee, J. Smith, G. Pagano, I.-D. Potirniche, A. C. Potter, A. Vishwanath, N. Y. Yao, and C. Monroe, *Nature (London)* **543**, 217 (2017).
- [12] C. Monre, W. C. Campbell, E. E. Edwards, R. Islam, D. Kafri, S. Korenblit, A. Lee, P. Richerme, C. Senko, and J. Smith, in *Proceedings of the International School of Physics of Physics "Enrico Fermi"*, edited by M. Knoop, I. Marzoli, and G. Morigi (IOS Press, Amsterdam, 2015), pp. 169–187.
- [13] R. Blatt and C. F. Roos, *Nat. Phys.* **8**, 277 (2012).
- [14] S. Schlemmer, T. Kuhn, E. Lescop, and D. Gerlich, *Int. J. Mass Spectrom.* **185**, 589 (1999).
- [15] S. Schlemmer, E. Lescop, J. von Richthofen, D. Gerlich, and M. A. Smith, *J. Chem. Phys.* **117**, 2068 (2002).
- [16] J. O. Hirschfelder, C. F. Curtiss, and R. B. Bird, *Molecular Theory of Transport in Gases* (Wiley, New York, 1954).
- [17] F. R. W. McCourt, J. J. M. Beenakker, W. E. Köhler, and I. Kuscer, *Nonequilibrium Phenomena in Polyatomic Gases* (Clarendon Press, New York, 1991), Vol. 2.
- [18] V. M. Zhdanov, *Transport Processes in Multicomponent Plasma* (Taylor and Francis, London, 2002).
- [19] S. Montero and Pérez-Ríos, *J. Chem. Phys.* **141**, 114301 (2014).
- [20] T. Stoecklin, P. Halvick, M. A. Gannouni, M. Holchaf, S. Kotochigova, and E. R. Hudson, *Nat. Commun.* **7**, 11234 (2016).
- [21] M. Tacconi, F. A. Gianturco, E. Yurtsever, and D. Caruso, *Phys. Rev. A* **84**, 013412 (2011).
- [22] D. Hauser, S. Lee, F. Carelly, S. Spieler, O. Lakhmanskaya, E. S. Endres, S. S. Kumar, F. Gianturco, and Wester, *Nat. Phys.* **11**, 467 (2015).
- [23] T. Stoecklin and A. Voronin, *Phys. Rev. A* **72**, 042714 (2005).
- [24] T. Stoecklin and A. Voronin, *Eur. Phys. J. D* **46**, 259 (2008).
- [25] T. Stoecklin and A. Voronin, *J. Chem. Phys.* **134**, 204312 (2011).
- [26] J. Pérez-Ríos and F. Robicheaux, *Phys. Rev. A* **94**, 032709 (2016).
- [27] A. Krüchow, A. Mohammadi, A. Härter, J. H. Denschlag, J. Pérez-Ríos, and C. H. Greene, *Phys. Rev. Lett.* **116**, 193201 (2016).
- [28] J. Pérez-Ríos and C. H. Greene, *J. Chem. Phys.* **143**, 041105 (2015).
- [29] C. H. Greene, P. Giannakeas, and J. Pérez-Ríos, *Rev. Mod. Phys.* **89**, 035006 (2017).
- [30] M. Karplus, R. N. Porter, and R. D. Sharma, *J. Chem. Phys.* **43**, 3259 (1965).
- [31] D. G. Truhlar and J. T. Muckerman, in *Atom-Molecule Collision Theory: A Guide for the Experimentalist* (Plenum Press, New York, 1979), pp. 505–561.
- [32] J. Pérez-Ríos, S. Ragole, J. Wang, and C. H. Greene, *J. Chem. Phys.* **140**, 044307 (2014).
- [33] Here  $r = r_{12}$  based on Fig. 1.
- [34] Another possible channel is the charge exchange process, in which  $\text{BaRb}^+ + \text{Rb} \rightarrow \text{BaRb} + \text{Rb}^+$ , although not considered here.
- [35] L. Bonnet and J. C. Rayez, *Chem. Phys. Lett.* **277**, 183 (1997).
- [36] W. H. Press, S. A. Teukolsky, W. T. Vetterling, and B. P. Flannery, *Numerical Recipes in Fortran 77* (Cambridge University Press, Cambridge, England, 1986).
- [37] C. Strauss, T. Takekoshi, F. Lang, K. Winkler, R. Grimm, J. Hecker Denschlag, and E. Tiemann, *Phys. Rev. A* **82**, 052514 (2010).
- [38] For the initial state  $r = r_{12}$  (see Fig. 1).
- [39] J. M. Bowman, *Mol. Phys.* **112**, 2516 (2014).
- [40] R. D. Levine and R. B. Bernstein, *Molecular Reaction Dynamics and Chemical Reactivity* (Oxford University Press, Oxford, 1987).
- [41] Here  $\tau_c = b_L/v_k$ , where  $b_L = (4C_4/E_k)^{1/4}$  is the Langevin impact parameter and  $v_k$  represents the collision velocity.